Error Estimation for ORION Baseline Vector Determination

S. C. Wu
Tracking Systems and Applications Section

Effects of error sources on ORION baseline vector determination are studied. Partial derivatives of delay observations with respect to each error source are formulated. Covariance analysis is then performed to estimate the contribution of each error source to baseline vector error. System design parameters such as antenna sizes, system temperatures and provision for dual-frequency (S- and X-band) operation are discussed.

I. Introduction

System design of an Operational Radio Interferometry Observing Network (ORION) is underway. The basic network will consist of a base station having a relatively large antenna and a mobile station having a smaller antenna. Nominal operating frequencies will be at X-band with a span bandwidth of up to 400 MHz. Among the cost-effective parameters to be designed are the antenna sizes, system temperatures and the provision for S- and X-band operation for possible need of charged media calibration. To understand how these parameters will affect the ultimate baseline measurement accuracy, the effects not only of these parameters but of all other possible error sources need to be studied. This article provides a covariance analysis to give an estimate of the effects of each individual error source. The ultimate baseline determination accuracy is estimated by taking the root-sum-square (rss) of the effects from all error sources. Baseline lengths of from 300 km to 5000 km are to be considered. Both 3-D baseline vector accuracy and baseline length accuracy are to be estimated.

II. Delay Observation

The information for the solution of baseline vector is derived from delay observations, over the baseline, of extragalactic radio sources (EGRS). The error-free information content of a single observation can be written as

$$\tau = -B_x \cos\delta \sin HA - B_y \cos\delta \cos HA + B_z \sin\delta \quad (1)$$

where δ = EGRS declination angle, HA = EGRS hour-angle at baseline center, B_x, B_y, B_z = baseline components with B_z parallel to the Earth's spin axis, B_x perpendicular to the meridian plane at baseline center and B_y completing a right-hand Cartesian coordinate system as shown in Fig. 1, and τ is delay over the baseline in km.

To determine the three baseline components at least three observations with non-coplanar lines-of-sight are needed, with orthogonal observations (perpendicular lines-of-sight) being optimum (in the sense of decoupling the three baseline components from one another).

In general, observations are sensitive to such systematic parameters as epoch offset, frequency drift, etc. Such sensitivity can be alleviated by including these parameters as additional estimated parameters (Ref. 1). Furthermore, it is well known that the sensitivity of a solution vector to observation error decreases as the number of independent observations increases. On the other hand, increasing the number of independent observations increases the total observation time and the data volume to be processed. Hence a compromise needs to be made.

When the number of observations is greater than three, the optimum combination is such that the direction vectors of the EGRS being observed have equal spreads in all three orthogonal directions. On the other hand, the availability of EGRS within a viewing window is limited. Specifically, the 14 sources listed

in Table 1 have been found to have correlated flux densities higher than 4 Janskys at X-band over a 300-km baseline. Hence an optimum observation sequence is not always attainable. A near optimum sequence, however, may be approached by proper scheduling. Table 2 is an observation sequence out of the 14 sources over a 24-hour period. Any 6-hour subset of this sequence provides a reasonable coverage of source position vectors in any three orthogonal directions. The sequence is in terms of the mean right ascension (RA) of the baseline center. The nominal observation time is 12 minutes except for the two sources having flux densities higher than 20 Janskys for which 4-minute observation time is allotted. A 1°/sec antenna slew rate has been assumed without considering cable wrapup allowances.

III. Covariance Analysis

The sensitivities of a delay observation to a perturbation of the baseline vector components are the partial derivatives of Eq. (1) with respect to these components:

$$\left\{\frac{d\tau}{dB_{x,y,z}}\right\} = \begin{bmatrix} \frac{\partial\tau}{\partial B_x} \\ \frac{\partial\tau}{\partial B_y} \\ \frac{\partial\tau}{\partial B_z} \end{bmatrix} = \begin{bmatrix} -\cos\delta \sin HA \\ -\cos\delta \cos HA \\ \sin\delta \end{bmatrix} \tag{2}$$

It is felt that perturbations in the length L and in the lateral LT and vertical VT directions of a baseline would provide better physical meaning than those in B_x, B_y and B_z. The partial derivatives of a delay observation with respect to these three physically meaningful components of a baseline can be derived from Eq. (2) with the aid of the following transformation matrix, which is straightforward in view of Fig. 2:

$$\left[\frac{\partial B_{x,y,z}}{\partial B_{L,LT,VT}}\right] = \begin{bmatrix} \frac{\partial B_x}{\partial B_L} & \frac{\partial B_x}{\partial B_{LT}} & \frac{\partial B_x}{\partial B_{VT}} \\ \frac{\partial B_y}{\partial B_L} & \frac{\partial B_y}{\partial B_{LT}} & \frac{\partial B_y}{\partial B_{VT}} \\ \frac{\partial B_z}{\partial B_L} & \frac{\partial B_z}{\partial B_{LT}} & \frac{\partial B_z}{\partial B_{VT}} \end{bmatrix}$$

$$= \begin{bmatrix} \cos\Omega & -\sin\Omega & 0 \\ \sin\Omega\sin\phi & \cos\Omega\sin\phi & -\cos\phi \\ \sin\Omega\cos\phi & \cos\Omega\cos\phi & \sin\phi \end{bmatrix} \tag{3}$$

where ϕ is the latitude of the baseline center and Ω is the lateral orientation angle of the baseline from due east. Hence

$$\left\{\frac{d\tau}{dB_{L,LT,VT}}\right\} = \left[\frac{\partial B_{x,y,z}}{\partial B_{L,LT,VT}}\right]^T \left\{\frac{d\tau}{dB_{x,y,z}}\right\}$$

$$= \begin{bmatrix} -\cos\delta\,(\sin HA\cos\Omega + \cos HA\sin\Omega\sin\phi) \\ \qquad + \sin\delta\sin\Omega\cos\phi \\ \cos\delta\,(\sin HA\sin\Omega - \cos HA\cos\Omega\sin\phi) \\ \qquad + \sin\delta\cos\Omega\cos\phi \\ \cos\delta\cos HA\cos\phi + \sin\delta\sin\phi \end{bmatrix} \tag{4}$$

As mentioned in Section II, effects of clock parameters can be alleviated by estimating these parameters. These include the epoch offset T_o and as many as 12 segments of clock rate offsets, $f_1, f_2, \ldots f_{12}$. The sensitivities of a delay observation to these parameters can easily be formulated: Let f_n applies to observations within the time segment $t_{n-1} < t < t_n$; then the sensitivities of a delay observation to these additional parameters within this time segment are

$$\frac{\partial\tau}{\partial T_o} = c \tag{5}$$

and

$$\frac{\partial\tau}{\partial f_i} = \begin{cases} c(t_i - t_{i-1}) & , \ i < n \\ c(t - t_{n-1}) & , \ i = n \\ 0 & , \ i > n \end{cases} \tag{6}$$

where c is the velocity of light.

For the solutions of N_e estimated parameters from M independent delay observations, an $N_e \times N_e$ information

matrix $J = A^T WA$ can be constructed the inverse of which is the computed covariance matrix

$$P_x = J^{-1} = (A^T WA)^{-1} \tag{7}$$

Here, A is an $M \times N_e$ sensitivity matrix with elements calculated according to Eqs. (4) – (6) for the M observations; W is an $M \times M$ diagonal weighting matrix with $W_{mm} = \sigma^{-2}_{\tau,m}$, the inverse of the error variance of the m^{th} delay observation. The diagonal elements of the computed covariance matrix (7) are the variances of the estimated parameters due to random errors in delay observations. Such errors include the effects of system noise and *random* tropospheric and ionospheric delay errors. Effects of *systematic* errors, such as atmospheric delay model errors, clock instability and source position errors, can be accounted for by including these parameters as "consider" parameters. The covariance matrix due to such systematic errors is given (Ref. 2) by

$$P'_x = P_x A^T WCP_c C^T WAP_x \tag{8}$$

where P_c is the covariance matrix of the N_c consider parameters and C is the sensitivity matrix to these parameters of the M delay observations.

Platform parameter errors (polar motion, UT1) and antenna location error are directly related to baseline vector error independent of observation sequence. Hence no covariance analysis of such errors is necessary.

Note that the effects of each *individual* error source on baseline vector components are of interest. These are calculated one at a time by setting all other error sources to be zero.

IV. Error Sources

This section calculates the variances σ_τ^2 of a delay observation due to random error sources and the sensitivities of the observation to systematic error sources. The variances σ_τ^2 will be used to construct the weighting matrix W in Eq. (7) and the sensitivities will be used in the construction of sensitivity matrix C in Eq. (8). Covariance matrices can then be calculated. The errors in the three baseline components are, respectively, given by the square roots of the first three diagonal elements of the corresponding covariance matrix. The following paragraphs study the effects of each error source.

A. System Noise

Delay observation error due to the system noise in the receiver front ends at the two sites of a baseline can be derived from Ref. 3 as[1]

$$\sigma_\tau = \frac{\sqrt{2}\,c}{2\pi f_{span}} \frac{1}{2.05 \times 10^{-4} SD_1 D_2} \left(\frac{T_{s,1} T_{s,2}}{e_1 e_2 BT} \right)^{1/2} \tag{9}$$

where

c = speed of light

f_{span} = span bandwidth, Hz

D_i = antenna diameter at site i, m

$T_{s,i}$ = system noise temperature at site i, K

B = channel bandwidth, Hz

e_i = antenna efficiency at site i

S = correlated flux density of EGRS, Janskys

T = observation (integration) time, sec

This is a random error and its effects on baseline vector components are calculated from the computed covariance matrix of Eq. (7).

B. Ionosphere

Ionospheric error can be divided into two types, systematic and random. Systematic error is a mismodeling error which can be expressed as

$$\sigma_\tau = [f(X_1) g(\gamma_1) - f(X_2) g(\gamma_2)]\ \epsilon_{peak} \tag{10}$$

where $f(X_i)$ and $g(\gamma_i)$ are the solar-zenith-angle factor and elevation-angle factor of site i, and ϵ_{peak} is the modeling error of the ionospheric peak at zenith. The solar-zenith-angle factor can be represented by the empirical function

$$f(X) = 0.2 + 0.8 \cos^{2/3} X \tag{11}$$

and the elevation-angle factor is given by (Ref. 4)

$$g(\gamma) = \{[(R_e + h_2)^2 - R_e^2 \cos^2 \gamma]^{1/2} - [(R_e + h_1)^2 - R_e^2 \cos^2 \gamma]^{1/2}\}/(h_2 - h_1) \tag{12}$$

[1] A "fudge factor" of 0.8 has been included to account for possible imperfect bandpass overlap and data processing loss.

where R_e = 6370 km, h_1 = 215 km and h_2 = 454 km.

Random ionospheric error is the result of fluctuations from the nominal values which can be represented by

$$\sigma_\tau = \frac{1}{2}\,[f(X_1)\,g(\gamma_1) + f(X_2)\,g(\gamma_2)]\;\epsilon'_{peak} \qquad (13)$$

where ϵ'_{peak} is the standard deviation of the peak zenith fluctuation difference between the two sites.

C. Troposphere

Both dry and wet components of tropospheric error can be divided into systematic and random parts. Systematic error can be written as

$$\sigma_\tau = \left(\frac{\epsilon^2_{z,1}}{\sin^2\gamma_1} + \frac{\epsilon^2_{z,2}}{\sin^2\gamma_2}\right)^{1/2} \qquad (14)$$

where $\epsilon_{z,i}$ is the zenith tropospheric calibration error at site i.

Random tropospheric error due to inhomogeneity can be written as

$$\sigma_\tau = \left(\frac{1}{\sin^2\gamma_1} + \frac{1}{\sin^2\gamma_2}\right)^{1/2} \epsilon'_z \qquad (15)$$

where ϵ'_z is the 1-σ standard deviation of the zenith fluctuation on each site.

D. Clock Instability

The effect of imperfect clocks on a delay observation is directly related to the difference between the drifts of the two clocks. It consists of an epoch offset and a relative drift. Epoch offset is an estimated parameter which is well isolated from baseline vector components and needs no further discussion. Clock drift effect is of a flicker random noise (as integrated over an observation time of ~12 minutes). It differs from a white random noise in that its Allan variance remains constant over all integration time instead of a linear decrease with integration time as for white random noise. Hence its effects cannot be treated as random effects. Instead, it is to be considered as systematic. The sensitivities of delay observations to such error can be simulated by a simple flicker noise model:

$$\sigma_{\tau,m} = f(N_m)\left[\left(\frac{\Delta f}{f}\right)^2_1 + \left(\frac{\Delta f}{f}\right)^2_2\right]^{1/2} c(\Delta t) \qquad (16)$$

where $(\Delta f/f)^2_i$ is the Allan variance of the clock at site i and $f(N_m)$ is a discrete function, at sampling time Δt, simulating a flicker noise of unity Allan variance given by the following recurrence formula:

$$f(j) = 1.95\,f(j-1) - 0.95\,f(j-2)$$

$$+\frac{1}{0.74}\left[\sum_{m=1}^{100} m^{0.6}\,g_{j+1-m} - 1.95\sum_{m=1}^{99} m^{0.6}\,g_{j-m}\right.$$

$$\left. + 0.95\sum_{m=1}^{98} m^{0.6}\,g_{j-1-m}\right] \qquad (17)$$

with g_j being the j^{th} sample of a Gaussian random number of unity standard deviation and $g_j = 0$ for $j < 1$. For a 60-sec sampling time N_m becomes the time of observation in minutes rounded to the nearest integer.

E. Source Positions

The angular position error of any single EGRS can be considered to be fixed. The right ascension and declination components of this error are assumed to be uncorrelated to and independent of each other and of any other sources. Hence the effects of each component of a source should be treated as an independent consider parameter and yet the effects of all sources can be included in a single estimation.

The sensitivities of a delay observation to the right-ascension and declination errors of an EGRS can be formulated from Eq. (1):

$$\frac{\partial\tau}{\partial\alpha} = B_x\cos\delta\cos HA - B_y\cos\delta\sin HA$$

$$\frac{\partial\tau}{\partial\delta} = B_x\sin\delta\sin HA + B_y\sin\delta\cos HA + B_z\cos\delta \qquad (18)$$

F. Polar Motion and UT1

The effects of polar motion error and of UT1 error on a baseline are independent of observation sequence and need no covariance analysis for their determination. It has been readily shown (Ref. 5) that x- and y-components of polar motion

error can be translated into the following baseline component errors:

$$\epsilon_{B_x} = \frac{-B_z}{a}\epsilon_x$$

$$\epsilon_{B_y} = \frac{B_z}{a}\epsilon_y \qquad (19)$$

$$\epsilon_{B_z} = \frac{B_x}{a}\epsilon_x - \frac{B_y}{a}\epsilon_y$$

where a is the Earth's radius at the pole.

These can be translated, with the aid of Fig. 2, into errors in baseline length and in lateral and vertical directions:

$$\epsilon_{B_L} = 0$$

$$\epsilon_{B_{LT}} = \frac{B}{a}\cos\phi\ \epsilon_x \qquad (20)$$

$$\epsilon_{B_{VT}} = \frac{B}{a}[(\cos\Omega\sin\phi)\epsilon_x - (\sin\Omega)\epsilon_y]$$

Therefore, the effects of polar motion error will be on baseline orientation only; baseline length will not be affected.

The effects of UT1 error on baseline vector can be derived from Eq. (1). Let $B_x = B_e \cos\lambda$ and $B_y = B_e \sin\lambda$; then (1) can be rewritten as

$$\tau = -B_e \cos\delta \sin(HA + \lambda) + B_z \sin\delta\ . \qquad (21)$$

A perturbation in UT1 of ϵ_{UT1} corresponds to a perturbation in HA of $\omega_e\ \epsilon_{UT1}$ where ω_e is the Earth's spinning speed. Such error will result in an error in λ of equal magnitude but of opposite sign. In turn, an error in λ of $\epsilon_\lambda = -\omega_e \epsilon_{UT1}$ will result in errors in B_x and B_y of

$$\epsilon_{B_x} = \frac{\partial B_x}{\partial\lambda}\epsilon_\lambda \qquad (22a)$$

$$= \omega_e B_y \epsilon_{UT1}$$

and

$$\epsilon_{B_y} = \frac{\partial B_y}{\partial\lambda}\epsilon_\lambda \qquad (22b)$$

$$= -\omega_e B_x \epsilon_{UT1}.$$

As before, these can be translated into errors in baseline length and in lateral and vertical directions:

$$\epsilon_{B_L} = 0$$

$$\epsilon_{B_{LT}} = -\omega_e B \sin\phi\ \epsilon_{UT1} \qquad (23)$$

$$\epsilon_{B_{VT}} = \omega_e B \cos\Omega\cos\phi\ \epsilon_{UT1}$$

Therefore, UT1 error will affect only baseline orientation but not baseline length.

G. Antenna Location

Antenna location may vary from one visit to another. Such error in repeatability translates directly into baseline error.

H. Phase Accountability

This is a random phase variation in the receiver bandpass. Its effects on baseline are estimated in the same way as system noise effects.

V. Results

In this section, covariance analysis will be performed for the determination of a 300-km baseline at mid-latitude ($\phi = 35°$) with a sequence of 32 delay observations. Such 32-observation (~6-hr) sequence is picked out of Table 2. To examine the dependence on the observation sequence, the first of the 32 consecutive observations runs through Table 2. Baseline error due to each error source will then be shown as a function of the starting RA of the baseline center. The following assumptions are to be made:

Baseline: 300 km at $\phi = 35°$

Antenna diameters: 26 m (base)
3 m (mobile)

Antenna efficiencies: 50%

System temperatures: 40 K (base)
130 K (mobile)

Channel bandwidth: 2 MHz

Span bandwidth: 400 MHz

EGRS flux densities: As in Table 1

Observation times: As in Table 2

Phase accountability: 0.2 cm each site (phase calibration assumed)

Clock instability: $\Delta f/f = 10^{-14}$ (hydrogen maser)

Zenith dry tropospheric error: 0.5 cm each site (systematic)

Zenith wet tropospheric error[2]: $0.5/\sqrt{2}$ cm each site (systematic)
$0.5/\sqrt{2}$ cm each site (random)

Zenith ionospheric error: 10 cm peak (systematic)
2 cm difference per 1000 km (random)

Polar motion error: 30 cm

UT1 error: 0.6 msec

EGRS angular position error: $0.01''/\sqrt{2}$ in RA and dec

Antenna location error: 0.5 cm (mobile site only)

Figures 3–11 display the results of covariance analysis. Here only the resultants of 3-D baseline errors are shown. Their mean values are summarized in Fig. 12 together with the effects due to platform parameter errors and antenna location error. Also shown in Fig. 12 are the corresponding errors in baseline length. It is observed that baseline length error accounts for only 30% of the total (3-D) baseline error. When baselines of different length are considered, it is found that errors due to ionosphere, source positions, polar motion and UT1 increase nearly linearly with baseline length. Such errors are drawn cross-hatched in Fig. 12. Errors due to other error sources essentially remain the same for all baseline lengths. (Tropospheric errors may increase slightly due to lower elevation angles for longer baselines.)

VI. Discussions

The above analysis provides an estimate of the effects of each possible error source on baseline vector determination. However, such information may not be of direct benefit to system design. In particular, one would need to look into the requirements on front-end system temperatures and antenna sizes to meet a given overall precision. These two parameters are among a few that are cost effective and controllable in the ORION System design. Other error sources are limited by state-of-the-art capabilities: for instance, clock stability, media and platform parameter calibrations and the knowledge of EGRS angular positions. Both antenna sizes and system temperatures affect baseline vector determination through Eq. (9), the equation for system noise effect. The variation of such effect with antenna sizes and system temperatures will be studied, keeping all other effects unchanged. To account for reduced correlated flux densities over longer baselines and for full capability of 14 pairs of 2-MHz channels of the Mark III VLBI System, the following changes of parameters are assumed:

EGRS correlated flux densities: 2 Janskys for all sources.

Total channel bandwidth: 14 X 2 MHz per sideband.

Observation times: 10 min.

Figure 13 displays the effects of system noise as functions of antenna sizes. Three combinations of system temperatures are considered: 130 K/130 K, 40 K/130 K, and 40 K/40 K. The higher temperature refers to an uncooled receiver front end and the lower temperature to a cooled front end. The tick marks along the abscissa indicate typical combinations of antenna diameters in meters. The absolute maximum of the system noise effect is limited by the minimum fringe phase signal-to-noise ratio (SNR) below which phase tracking may fail. This corresponds to a baseline vector error of ~3.1 cm and a baseline length error of ~1.2 cm. This threshold is shown as a dashed line in Fig. 13.

For a base station with $D = 26$ meters and $T_S = 40$ K and a mobile station with $D = 3$ meters and $T_S = 130$ K, the system noise effects are found to be ~0.8 cm on baseline vector and ~0.3 cm on baseline length. These are comparable with the results shown in Fig. 12 for a 300-km baseline. It is observed that for such, and shorter, baseline lengths the effects of system noise are comparable with other error sources and consideration of antenna sizes and system temperatures may play an important role in overall baseline determination accuracy. For baselines longer than 300 km, those errors which are cross-hatched in Fig. 12 are to be scaled directly by baseline length[3]. Hence, for baselines 1000 km or longer, effects from ionosphere, source positions, polar motion and UT1 will dominate. It becomes relatively immaterial as to what combination of antenna sizes and system temperatures are used. This is illustrated in Figs. 14 and 15 for baseline vector error and baseline length error respectively. For a 5000-km baseline, the overall errors are effectively constant regardless of antenna sizes and system temperatures. Unless the knowledge of source positions, polar motion and UT1 can

[2] Assuming water vapor radiometers are used. Bias errors will appear as clock epoch error which is to be estimated.

[3] Error from troposphere will also increase slightly due to lower elevation angles for longer baselines.

be improved by a factor of ~3, consideration of antenna sizes and system temperatures is insignificant for baselines longer than 2000 km, as long as the signals are sufficiently strong to maintain a fringe phase SNR exceeding the minimum threshold.

The above study has been based on observations over an integration time of 600 sec. Of course, tradeoffs can be made between antenna sizes and observation time and between system temperatures and observation time: A decrease in observation time by a factor of 2 corresponds to a decrease in the product of antenna diameters by a factor of $\sqrt{2}$ or an increase in one of the system temperatures by a factor of 2. Therefore, antenna sizes greater than or system temperatures smaller than are needed to attain a specified precision allow a shorter integration time (and hence smaller data volume) per observation. Figures 13–15 can be used for integration times T other than 600 sec by simply moving the scale on the abscissa to the left by a factor $(600/T)^{1/2}$

In regard to Fig. 12, the S/X calibration of ionospheric error needs to be mentioned. With the projected capabilities of source-position, polar-motion and UT1 calibrations assumed, the effects on baseline *vector* determination of these errors are much higher than that of ionospheric error (with Faraday rotation calibration). The dominance of these errors over ionospheric error will remain for all baseline lengths since they all increase with baseline length. Hence the need of S/X calibration does not seem justified unless the knowledge of source positions, polar motion and UT1 can be improved. This statement is not true in the case of baseline *length* determination since polar motion and UT1 do not affect its accuracy as shown in the lower part of Fig. 12. Ionospheric error without S/X calibration becomes a major error souce in the determination of baseline *length* 1000 km or longer.

References

1. MacDoran, P. F., et al., "Radio Interferometric Geodesy Using a Rubidium Frequency System," Proc. of the 7th Annual Precision Time and Time Interval (PTTI) Applications and Planning Meeting, Goddard Space Flight Center, Greenbelt, Maryland, December 2-4, 1975, pp. 439-454.
2. Bierman, G. J., *Factorization Methods for Discrete Sequential Estimation*, Academic Press, 1977, Chapter 8.
3. Thomas, J. B., *An Analysis of Long Baseline Radio Interferometry, Part II*, Technical Report 32-1526 Vol. VIII, Jet Propulsion Laboratory, Pasadena, Calif., April 1972, pp. 29-38.
4. Liu, A., and Cain, D., *Ionospheric Range and Angular Corrections*, Technical Memorandum, 312-694, Jet Propulsion Laboratory, Pasadena, Calif., March 1966.
5. Williams, J. G., "Very Long Baseline Interferometry and Its Sensitivity to Geophysical and Astronomical Effects," *Space Program Summary 37-62, Vol. II*, Jet Propulsion Laboratory, Pasadena, Calif., March 1970, pp. 49-54.

Table 1. X-band VLBI extragalactic radio sources

Source	Right-ascension	Declination	Correlated flux density over 300-km baseline,[a] Janskys
3C 84	49.12°	41.33°	44.6
DA 193	88.01	39.81	5.2
P 0605-08	91.40	-8.57	4.5
OJ 287	132.99	20.30	4.7
4C 39.25	140.98	39.26	7.8
3C 273	186.64	2.33	32.5
3C 279	193.40	-5.52	12.2
3C 345	250.32	39.90	6.8
NRAO 530	262.56	-13.05	5.1
P 1741-038	265.34	-3.81	5.6
OV -236	290.87	-29.28	6.8
3C 418	309.28	51.14	5.6
P 2134+004	323.72	.47	8.0
3C 454.3	342.87	15.88	6.3

[a]Correlated flux density may vary with time; for the current analysis, however, these crude estimates can be used without introducing unrealistic error.

Table 2. ORION 24-hour observation sequence

Source	T_{obs}	Right-ascension of baseline center hr	min	sec
DA 193	12	0	0	0
3C 84	4	0	8	29
3C 454.3	12	0	17	31
P 2134+004	12	0	29	55
3C 418	12	0	42	47
3C 84	4	0	51	51
DA 193	12	1	0	20
P 2134+004	12	1	14	15
3C 454.3	12	1	26	39
3C 418	12	1	39	23
3C 84	4	1	48	27
DA 193	12	1	56	56
P 0605-008	12	2	9	44
3C 84	4	2	18	47
3C 454.3	12	2	27	49
P 0605-08	12	2	41	39
3C 418	12	2	55	46
3C 84	4	3	4	50
P 0605-08	12	3	13	53
4C 39.25	12	3	26	59
3C 84	4	3	36	5
DA 193	12	3	44	34
OJ 287	12	3	57	17
P 0605-08	12	4	10	7
3C 84	4	4	19	10
DA 193	12	4	27	39
OJ 287	12	4	40	22
4C 39.25	12	4	52	42
P 0605-08	12	5	5	48
3C 84	4	5	14	51
P 0605-08	12	5	23	54
DA 193	12	5	36	42
OJ 287	12	5	49	25
P 0605-08	12	6	2	15
3C 84	4	6	11	18
DA 193	12	6	19	47
P 0605-08	12	6	32	35
4C 39.25	12	6	45	41
OJ 287	12	6	55	1
DA 193	12	7	10	44
P 0605-08	12	7	23	32
3C 84	4	7	32	35
OJ 287	12	7	41	47
4C 39.25	12	7	54	7
P 0605-08	12	8	7	13
3C 273	4	8	16	49
3C 84	4	8	22	51
OJ 287	12	8	32	3
3C 84	4	8	41	15
3C 279	12	8	51	27
3C 273	4	8	59	37
P 0605-08	12	9	9	13
DA 193	12	9	22	1
OJ 287	12	9	34	44
4C 39.25	12	9	47	4
3C 273	4	9	55	59
3C 279	12	10	4	9
4C 39.25	12	10	17	15
3C 345	12	10	30	33
3C 273	4	10	39	42
OJ 287	12	10	48	37
3C 279	12	11	1	42
DA 193	12	11	15	27

Source	T_{obs}	Right-ascension of baseline center hr	min	sec
4C 39.25	12	11	28	7
3C 273	4	11	37	2
DA 193	12	11	46	37
3C 345	12	12	0	16
3C 279	12	12	13	25
3C 273	4	12	21	35
OJ 287	12	12	30	30
3C 279	12	12	43	35
4C 39.25	12	12	56	41
3C 279	12	13	9	47
3C 345	12	13	22	56
3C 273	4	13	32	5
P 1741-038	12	13	41	24
3C 418	12	13	54	30
3C 345	12	14	7	12
3C 279	12	14	20	21
NRAO 530	12	14	33	29
3C 279	12	14	46	37
3C 418	12	15	0	27
3C 345	12	15	13	9
3C 273	4	15	22	18
4C 39.25	12	15	31	13
NRAO 530	12	15	45	16
3C 345	12	15	58	10
P 1741-038	12	16	10	56
NRAO 530	12	16	23	6
3C 273	4	16	32	23
3C 418	12	16	42	11
P 1741-038	12	16	55	17
3C 345	12	17	8	3
NRAO 530	12	17	20	57
P 2134+004	12	17	33	59
OV -236	12	17	46	42
3C 454.3	12	17	59	49
OV - 236	12	18	12	56
3C 418	12	18	26	18
NRAO 530	12	18	39	34
3C 345	12	18	52	28
P 1741-038	12	19	5	14
3C 418	12	19	18	20
OV -236	12	19	31	42
P 2134+004	12	19	44	25
NRAO 530	12	19	57	27
3C 345	12	20	10	21
OV -236	12	20	23	40
3C 418	12	20	37	2
3C 454.3	12	20	49	46
OV -236	12	21	2	53
3C 418	12	21	16	15
3C 84	4	21	28	15
P 2134+004	12	21	41	7
3C 84	4	21	50	33
P 2134+004	12	21	59	59
3C 454.3	12	22	12	23
3C 345	12	22	25	45
3C 84	4	22	35	22
P 2134+004	12	22	44	48
3C 418	12	22	57	40
3C 454.3	12	23	10	24
P 2134+004	12	23	22	48
3C 418	12	23	35	40
P 2134+004	12	23	48	32

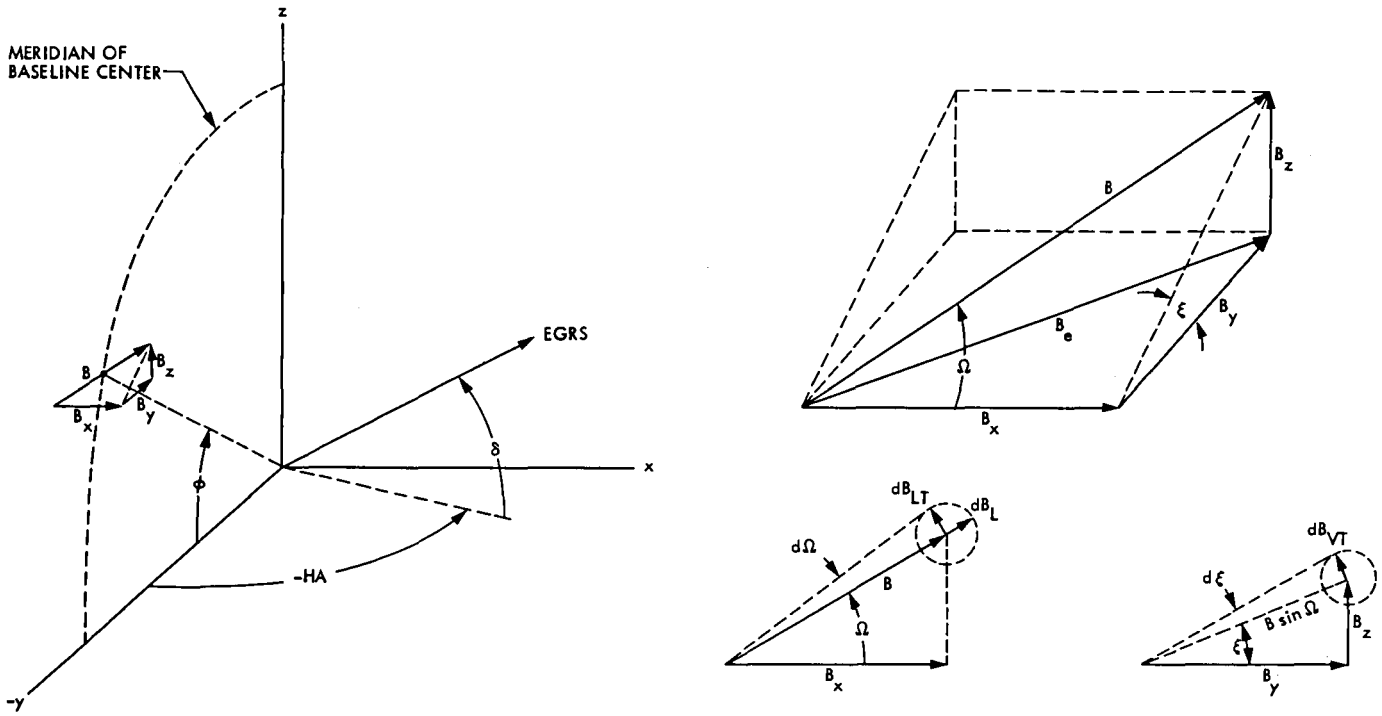

Fig. 1. Geometry of baseline and EGRS

$B_x = B \cos \Omega$ $\quad dB_L = dB$ (LENGTH)

$B_y = B \sin \Omega \cos \xi$ $\quad dB_{LT} = B\, d\Omega$ (LATERAL)

$B_z = B \sin \Omega \sin \xi$ $\quad dB_{VT} = B \sin \Omega\, d\xi$ (VERTICAL)

$\pi/2 - \xi = \phi$ = BASELINE CENTER LATITUDE

Fig. 2. Transformation of baseline component differentials

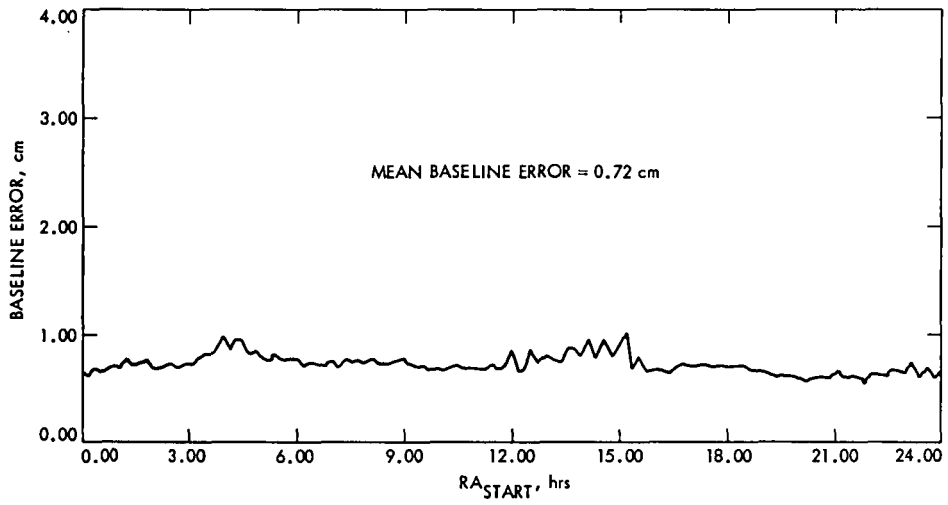

Fig. 3. System noise effects on baseline vector determination

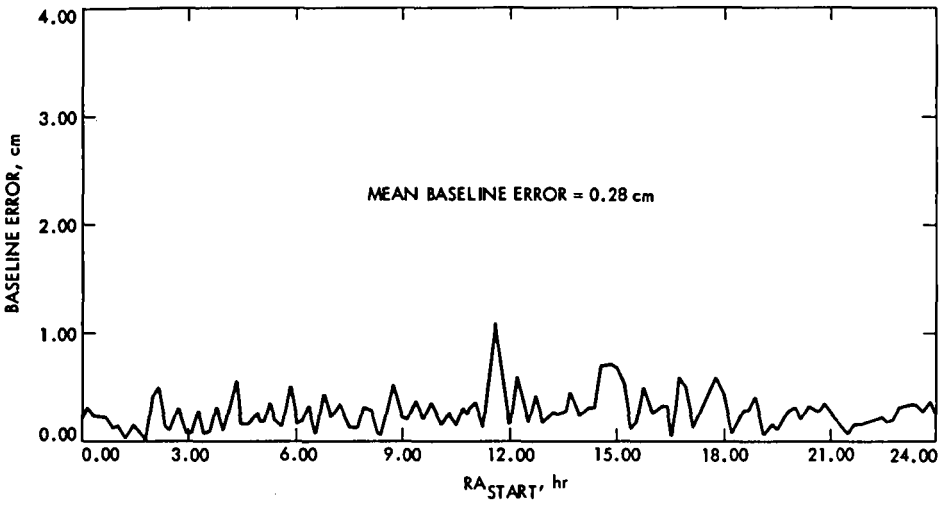

Fig. 4. Clock instability effects on baseline vector determination

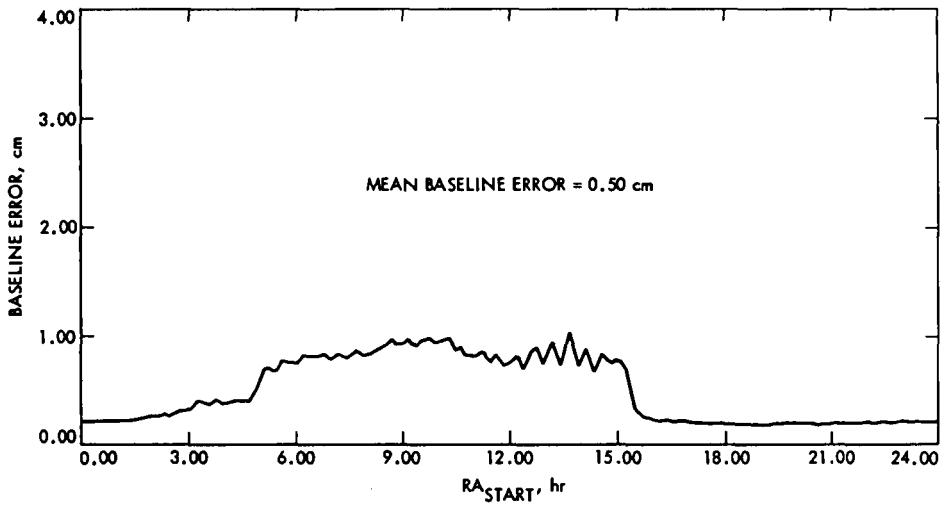

Fig. 5. Effects of systematic ionospheric error on baseline vector determination

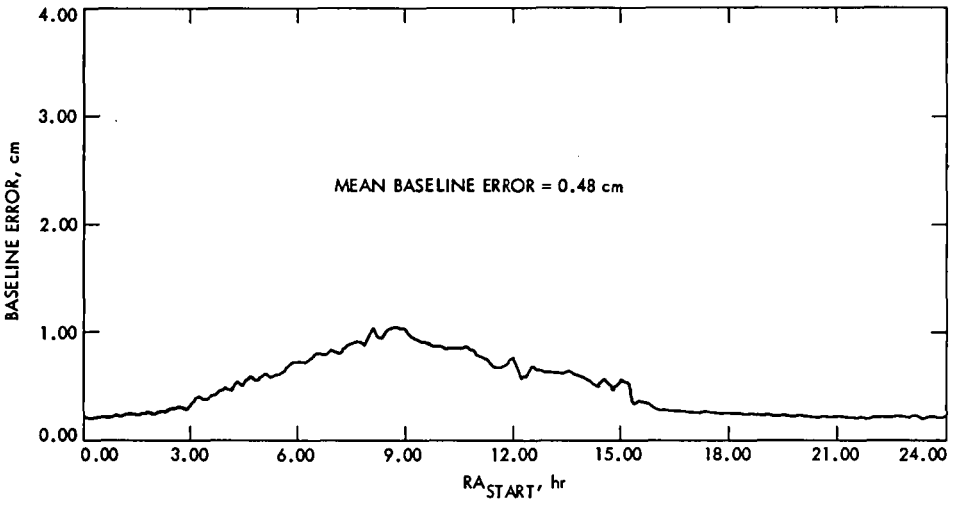

Fig. 6. Effects of random ionospheric error on baseline vector determination

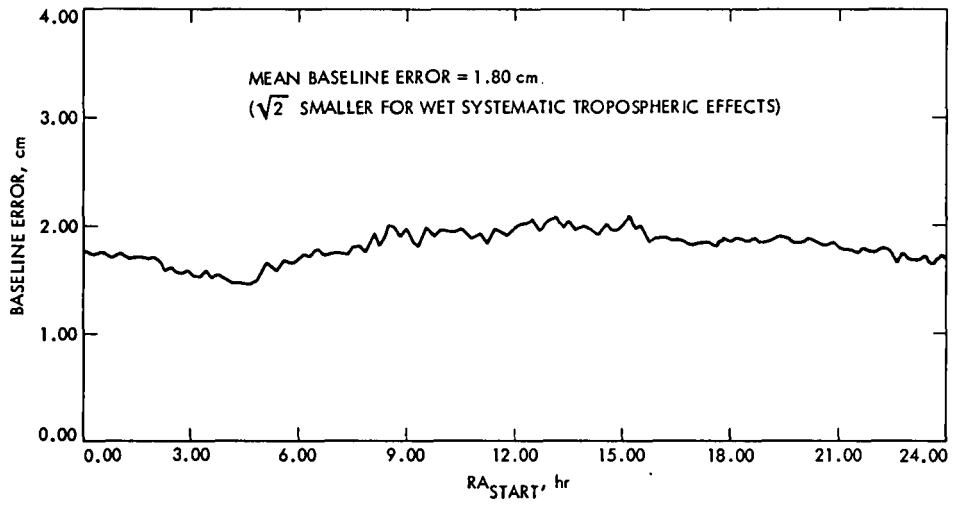

Fig. 7. Effects of dry tropospheric error on baseline vector determination

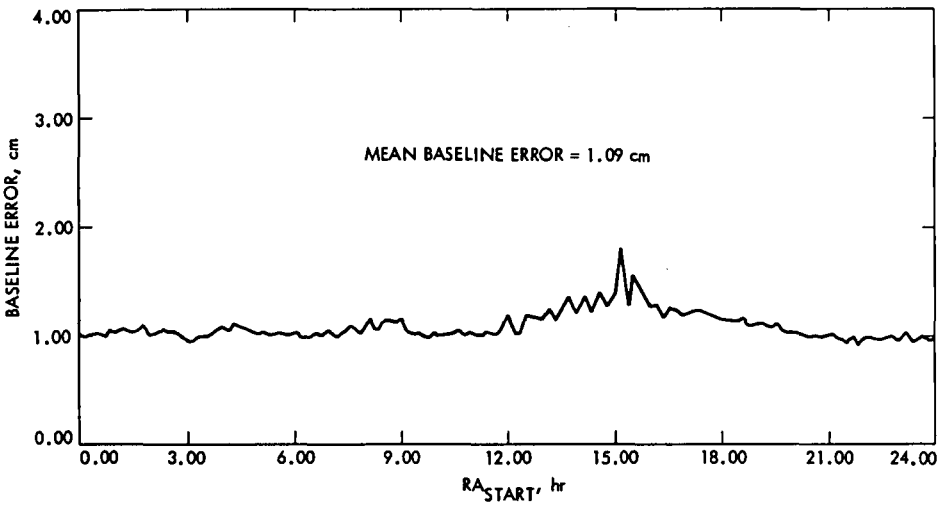

Fig. 8. Effects of random wet tropospheric error on baseline vector determination

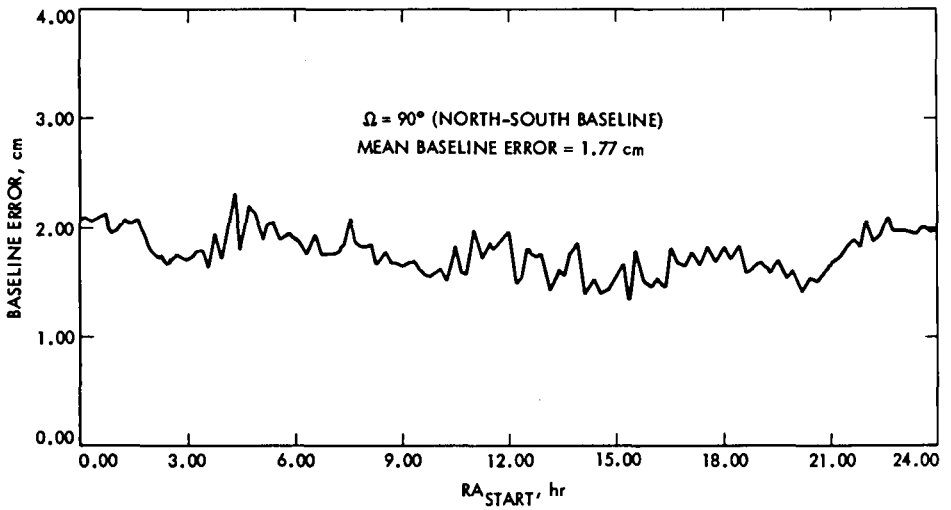

Fig. 9. Effects of EGRS position errors on baseline vector determination

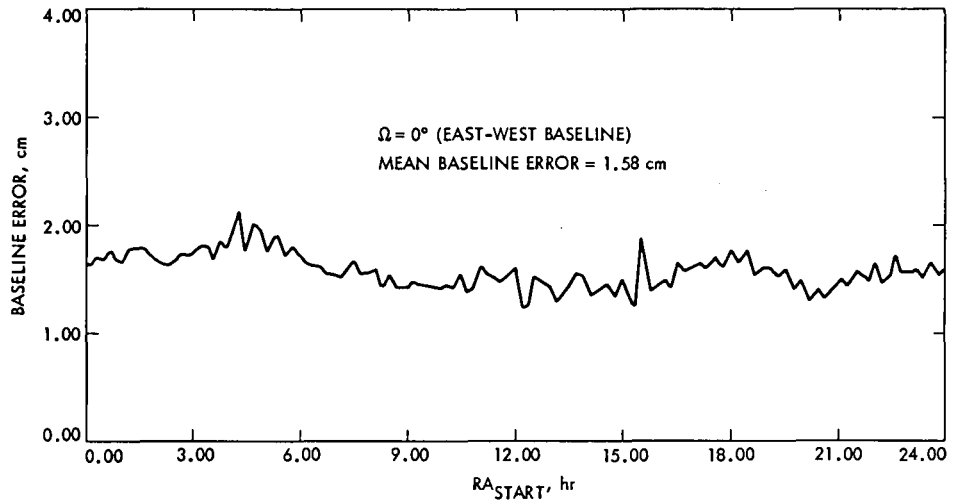

Fig. 10. Effects of EGRS position errors on baseline vector determination

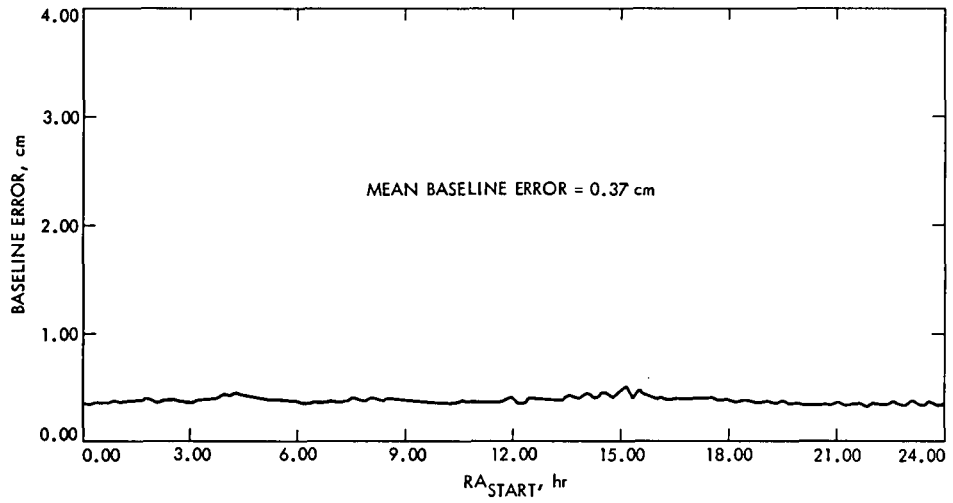

Fig. 11. Effects of system phase accountability error on baseline vector determination

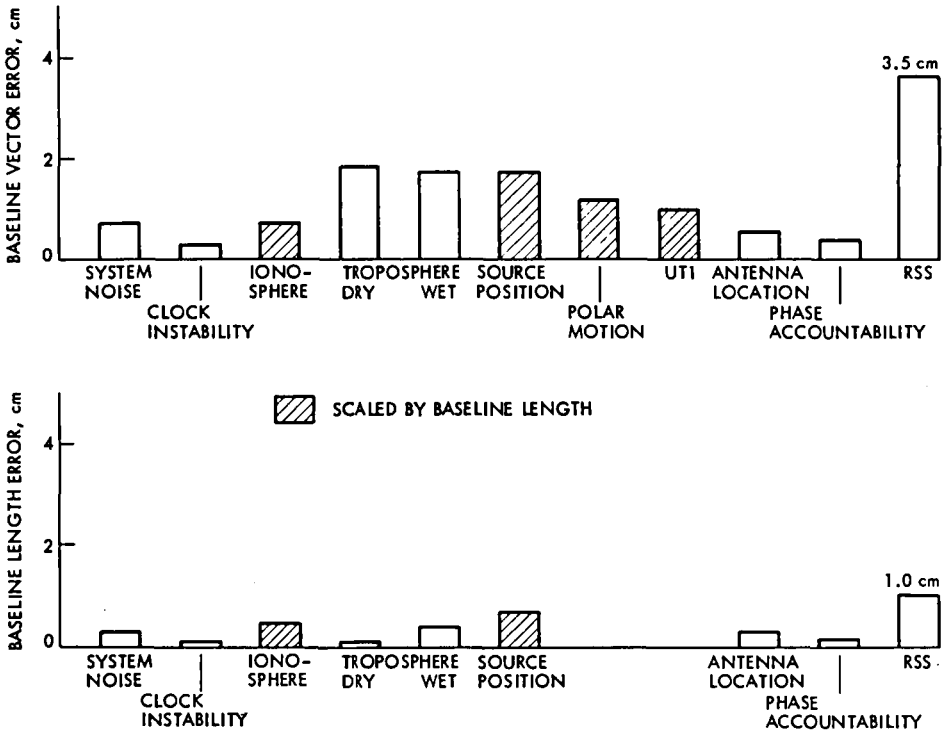

Fig. 12. Baseline vector and length determination errors

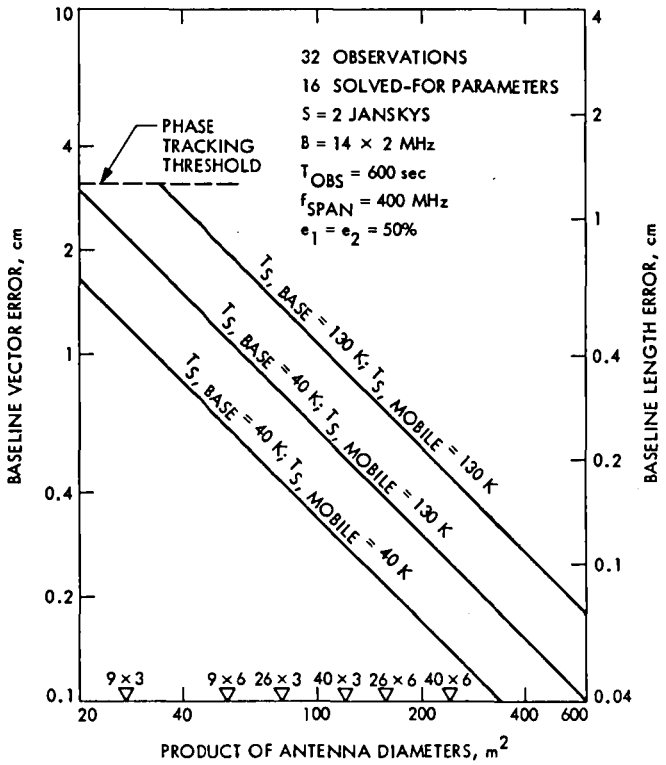

Fig. 13. Contribution of system noise to baseline determination error

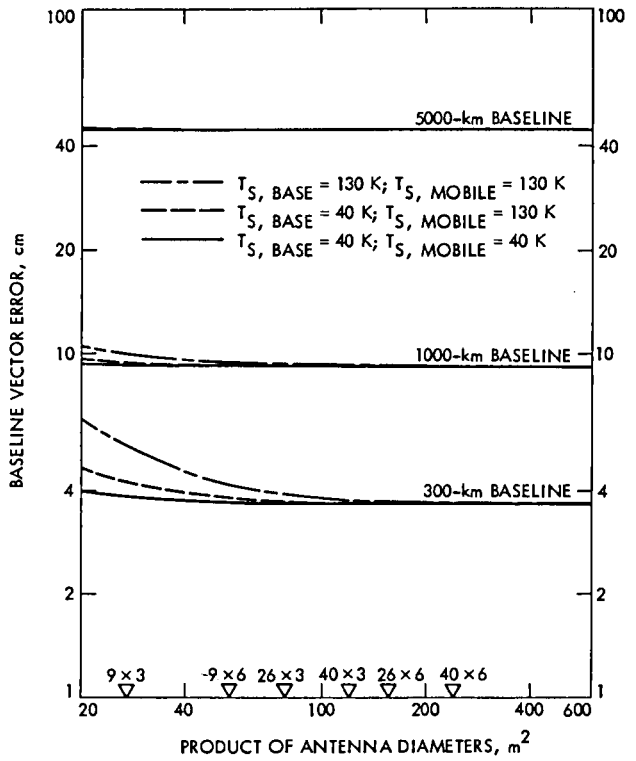

Fig. 14. Total baseline vector determination error

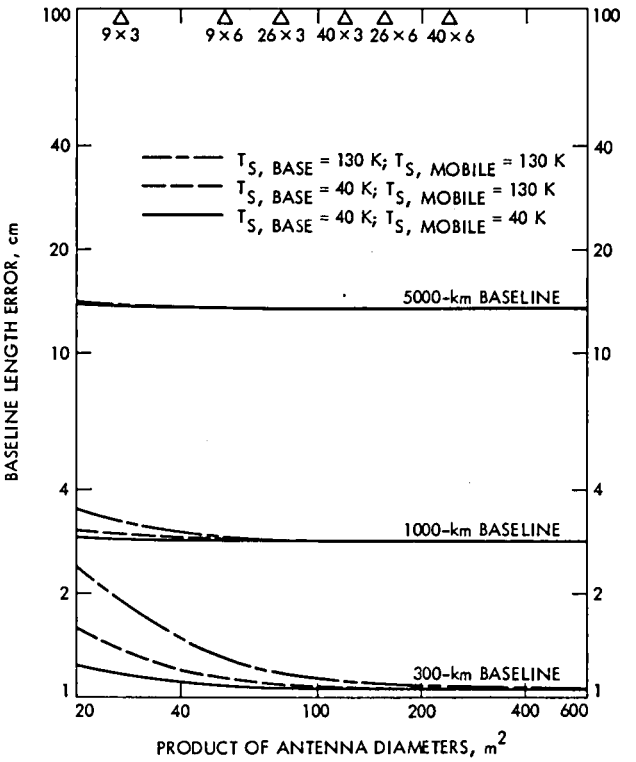

Fig. 15. Total baseline length determination error